Vibrationally resolved inelastic scattering and charge transfer in H+–C2H4 collisions

N. Aristov, W. Maring, G. NiednerSchatteburg, J. P. Toennies, Y.N. Chiu, and H. Köppel

Citation: The Journal of Chemical Physics **99**, 2682 (1993); doi: 10.1063/1.465230
View online: http://dx.doi.org/10.1063/1.465230
View Table of Contents: http://scitation.aip.org/content/aip/journal/jcp/99/4?ver=pdfcov
Published by the AIP Publishing

Vibrationally resolved inelastic scattering and charge transfer in H^+–C_2H_4 collisions

N. Aristov,[a] W. Maring, G. Niedner-Schatteburg,[b] and J. P. Toennies
Max-Planck-Institut für Strömungsforschung, Bunsenstr. 10, 3400 Göttingen, Germany

Y.-N. Chiu
Center for Molecular Dynamics and Energy Transfer, Department of Chemistry, The Catholic University of America, Washington DC 20064

H. Köppel
Institut für Physikalische Chemie, Universität Heidelberg, 6900 Heidelberg, Germany

(Received 30 December 1992; accepted 28 April 1993)

Differential cross sections and time-of-flight spectra have been measured in a crossed molecular beam apparatus for inelastic scattering and charge transfer in collisions of 30 eV protons with ethylene. High resolution inelastic time-of-flight spectra reveal peaks corresponding to the fundamentals of at least two of the infrared active antisymmetric vibrational modes of ethylene. In the time-of-flight spectra of H atoms resulting from charge transfer energy loss, peaks corresponding to excitation of two electronic states of the ethylene molecular ion are resolved. The H-atom product angular distributions are consistent with a 2.0 eV potential well in the ground state potential energy surface of the charge transfer reaction. The observations for the antisymmetric vibrational modes are explained in terms of an ion-induced dipole mechanism. Excitation of the symmetric modes is attributed to a vibronic coupling mechanism. An appendix provides a detailed account of the vibronic distributions in idealized low energy, high symmetry collisions leading to stable $C_2H_5^+$ complexes.

I. INTRODUCTION

State resolved vibrational inelastic scattering (IS) and charge transfer (CT) have been studied in collisions between 30 eV protons and the polyatomic molecule C_2H_4 using methods similar to those involved in proton energy loss spectroscopy (PELS).[1] The scattered protons and H atoms are detected as a function of time-of-flight and scattering angle. Because the protons are "structureless," the scattering distributions depend only on the nature of the interaction with the target molecule. In the previously studied small di- and triatomic systems[2,3] and the more recently reported CH_4 (Ref. 4) and C_2H_2 (Ref. 5) polyatomic molecules, vibronic final state levels could be clearly resolved for both inelastic and in some cases for charge transfer scattering, allowing a detailed interpretation in terms of the interaction dynamics. For example, in $H^+ + C_2H_2$, long range collisions at small scattering angles lead to excitation of the C–H bonds at the ends of the molecules, whereas in closer collisions at larger scattering angles the inelastic excitation of the inner C–C bond was more probable. A similar switching behavior with scattering angle was observed in the branching ratio between the inelastic and charge transfer scattering. A further result of the acetylene experiments was the observation of a vibrational mode of the $C_2H_2^+$ ion that had been only reported in an infrared spectrum[6] and, preliminarily, in a threshold photoionization study of C_2H_2 (Ref. 7).

The results for the proton-methane and -acetylene systems indicate that IS and CT involve mainly two types of mechanism operating at different ranges of impact parameters. The stronger interaction is a long range ion-induced dipole coupling which excites only the infrared active vibrational modes (induced dipole mechanism, IDM). The observation of infrared *in*active mode excitation as well as charge transfer implied that other mechanisms must also occur. The probability of these processes was observed to increase with scattering angle, corresponding to decreasing impact parameter and are therefore attributed to short range interactions. Qualitatively, these additional mechanisms can be attributed to bond dilution and bond angle distortion resulting from the redistribution of electron density in the molecule as it adopts a lower energy configuration in the presence of the perturbing proton. This temporary distortion naturally leads to vibrational excitation, and in extreme cases of electron density redistribution, to charge transfer. This mechanism is called the internal vibronic mechanism (IVM).

The above mechanisms differ from one another in that at long range, as mentioned above, the strongest distorting force is through the attraction between the ion and the induced dipole of the molecule, whereas at close range, additional forces pull the collision partners toward adopting the configuration of a $(C_nH_{m+1})^+$ complex. The latter can induce symmetric (infrared inactive) stretches of a bond or changing of a bond angle. This complex becomes important in the vicinity of a crossing of diabatic potential energy surfaces, where a branching between disintegration back to vibrationally excited reactants or to charge transfer products can occur. This branching ratio is determined by

[a]Present address: Institute for Chemical Education, Dept. of Chemistry, University of Wisconsin, Madison, WI 53706.
[b]Present address: Institute für Physikalische und Theoretische Chemie, Technische Universität München, Lichtenbergstrasse 4, 8046 Garching, Germany.

 0021-9606/93/99(4)/2682/13/$6.00

the strength of the coupling between the reactant and product surfaces, which is dependent on their vibronic symmetry.

It has been shown[5] that the energies corresponding to these couplings can be represented by matrix elements of the totally symmetric operator $Q \cdot \partial H_{el}/\partial Q$, where H_{el} is the electronic Hamiltonian including electronic kinetic and coulombic energies and Q is a normal mode coordinate in the collision complex. Thus, the strongest interactions will occur between modes that conserve the total vibronic symmetry in the reactants, collision complex, and products along the reaction coordinate. When Q is a molecular vibration, both infrared active and inactive modes can be excited; the transition probability for a given vibrational normal mode is dependent on its symmetry and on the symmetry of the electronic states involved. This has been used to deduce the equilibrium geometry of the complex and the ensuing vibrational excitation. This internal vibronic mechanism has also been likened to a "chemically induced Jahn–Teller effect."[8] Formally, this effect accounts for the fact that a molecule with degenerate states of high symmetry is unstable and will therefore distort to a lower symmetry to break the degeneracy. In our case the instability is introduced by the appearance of the proton, which causes a degeneracy between the two states $H^+\cdots C_nH_m$ and $H\cdots C_nH_m^+$ when it abstracts an electron from the target.

A third, quasimolecular mechanism (QMM) was also discussed in the CH_4 and C_2H_2 systems. In this case vibronic coupling through the pseudo Jahn–Teller effect, where the interacting surfaces may be several eV apart, is invoked.[9] In this mechanism the proton–molecule interaction is viewed from the opposite limit: Instead of the proton acting as a perturbation of the target molecular potential surfaces as in IVM, in QMM the $H^+\cdots C_nH_m$ system is taken as a single molecular complex. The symmetry arguments just presented are the same for both IVM and QMM. In this report we focus on the former and include a discussion of the strong-coupling QMM scheme in the Appendix.

Other channels, such as those proceeding via the first excited state of the ethylene ion

$$\begin{aligned} H^+ + C_2H_4 &\rightarrow [H-C_2H_4^+(\tilde{A})]^* \\ &\rightarrow H_2 + C_2H_3^+ \quad (4.9 \text{ eV exo}) \\ &\rightarrow H_2 + C_2H_2^+ + H \quad (0.4 \text{ eV exo}) \end{aligned}$$

are energetically available to this system. The analogous production of vinyl and acetylene ions has been observed in photoionization studies of ethylene.[10] There is only a small probability that the first channel can be detected in our apparatus. The second reaction could be observed if the H atom product had sufficient energy and were scattered in the forward direction. Its absence is probably due to the fact that the reaction requires three steps: charge transfer to make $C_2H_4^+$, radiationless decay to the ground state of the ethylene ion, followed by rearrangement and dissociation.[11]

TABLE I. Energies, intensities, and symmetries of the fundamental vibrational normal modes of C_2H_4. All energies are taken from Ref. 26. Intensities are experimental IR (for antisymmetric modes, in $cm^{-2}\,atm^{-1}$) and calculated Raman (for symmetric modes, in $Å^4\,amu^{-1}$) (Ref. 13).

Mode	Energy (meV)	Intensities	Symmetry
ν_1	375.0	4.9 R	a_g sym CH_2 stretch
ν_2	201.2	1.2 R	a_g sym C–C stretch
ν_3	166.4	1.7 R	a_g sym CH_2 scissor
ν_4	127.0		a_u twist
ν_5	384.7	4.5 R	b_{3g} sym C–H stretch
ν_6	153.2	0 R	b_{3g} sym rock
ν_7	117.6	330 IR	b_{3u} asym wag
ν_8	116.9	0.4 R	b_{2g} sym wag
ν_9	385.0	101 IR	b_{2u} asym C–H stretch
ν_{10}	102.4	0.8 IR	b_{2u} asym rock
ν_{11}	370.6	54.9 IR	b_{1u} asym CH_2 stretch
ν_{12}	179.0	39.6 IR	b_{1u} asym scissor

Table I lists the energies, symmetries, and infrared (IR) or Raman intensities as well as the motion of the vibrational modes of C_2H_4 for later reference.

The article starts with a brief description of the apparatus. The experimental results are discussed next. The dynamical approximations are discussed in Sec. IV. Finally the article closes with a brief conclusions section.

II. APPARATUS

The apparatus used in most of the experiments described here has already been described in detail elsewhere.[1,14] A mass and energy selected pulsed proton beam is crossed with an effusive, uncollimated target molecular beam. The scattered protons or H atoms are detected by the same electron multiplier as a function of the flight time at the end of a 2.93 m long flight tube. The protons are accelerated by the 3 kV potential of the first dynode of the multiplier. The proton detection efficiency is $\simeq 100\%$. For detecting H atoms, the proton signal is suppressed by application of a +200 V repelling field on a ring electrode inside the flight tube. At 30 eV H atoms also eject electrons from the first dynode of the multiplier but the detection efficiency of the hydrogen atoms is somewhere between 5% (Ref. 15) and 1%.[16] All the results for H-atom scattering shown here have been corrected by a factor of 20 so that the intensities can be compared at least approximately. In order to measure angular distributions, the proton source is rotated in the plane perpendicular to the secondary beam.

III. EXPERIMENTAL RESULTS

Figure 1 shows the angular distributions of all scattered protons and also those of the H atoms produced in charge transfer. Both distributions are peaked in the forward direction, decrease steeply towards larger angles and, unlike the previously studied CH_4 and C_2H_2, show no clear evidence for a rainbow maximum. Figure 1 indicates that the relative probability for CT is quite high, becoming more probable than IS already at $\theta \geqslant 1.5°$ and reaching three times the IS probability at $\theta = 6°$, above which the

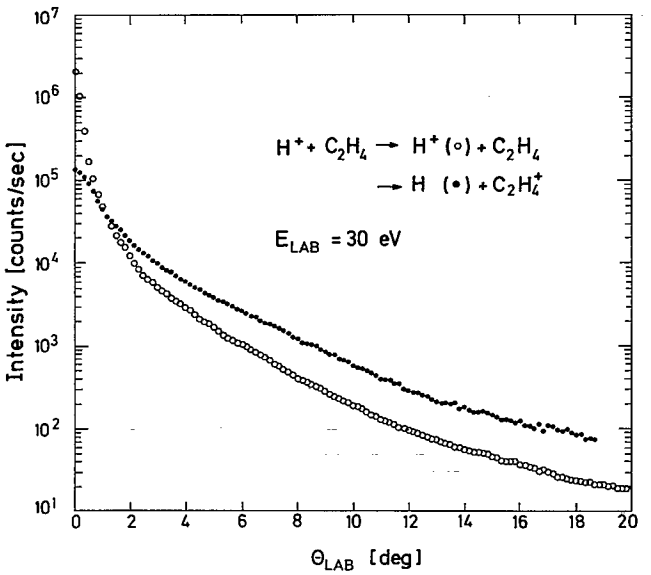

FIG. 1. Comparison of the total signal of protons (○) and H atoms (●) measured as a function of the laboratory scattering angle in the scattering of $H^+ + C_2H_4$ at 30 eV collision energy. The H atom intensities have been corrected to account for the lower detector sensitivity. Note that for angles greater than 1.5 degrees charge transfer is more probable than the total elastic and inelastic scattering of protons.

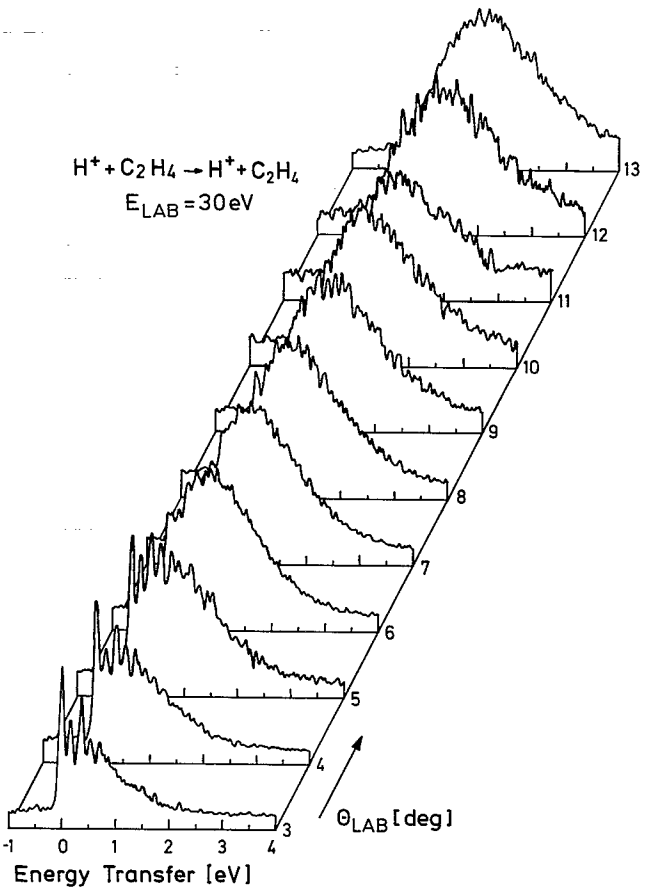

FIG. 2. Time-of-flight energy loss distributions for inelastic scattering at 30 eV at several scattering angles between $\theta = 3$ and 13°.

relative probability stays fairly constant. Methane showed no strong angular dependence in the CT/IS ratio and the probability of charge transfer was also larger, twice as high as that of IS. In acetylene, the angular dependence in the branching ratio was much larger but the highest relative CT probability was only 50%. The low CT efficiency in C_2H_2 was partially explained through severe symmetry restrictions, allowing in principle only certain collision geometries to lead to products. In methane and ethylene, the symmetry requirements appear to be less restrictive. A more important effect, however, is the fact that both methane and ethylene can undergo charge transfer in near-resonant processes, while in acetylene this reaction is very exothermic.

Figure 2 shows a series of energy loss spectra of protons measured at several scattering angles between $\theta = 3°$ and 13°. With increasing scattering angle, the amount of energy transfer increases and the spectrum becomes less structured. The maximum in the energy loss distribution also moves from $\Delta E = 0$ eV at 3° to $\Delta E \simeq 1.5$ eV at 13°. The spectra at low scattering angles $\theta \leqslant 5°$ show up to six resolved vibrational peaks with an apparent modulation in the peak heights. This alternation in the intensities of the peaks suggests that several different normal or combination modes are excited with varying probability. If one particular vibration were excited into a series of higher lying overtones then the intensities should show a smooth behavior. The first peak in all the spectra is primarily due to elastic scattering, the second peak to modes lying between 100 and 250 meV and the third to modes between 250 and 500 meV as well as overtones/combination bands of lower energy peaks. Since, as can be seen from Table I, all the normal modes of ethylene lie below $\simeq 400$ meV in energy the higher energy loss part of the spectrum can only be due to overtones or combination bands. The loss of resolution toward large scattering angles prevents comparing the relative excitation probabilities of various modes as was done for the acetylene system.[5] In that study, as mentioned in the Introduction, a quite interesting switchover from primarily C–H excitation at low angles to C–C excitation at high θ was observed.

Figure 3 shows very recent high resolution energy loss measurements at $\theta = 0°$ and $E = 20$ eV collision energy from a new apparatus in which electrostatic sector fields are used both as monochromator and as analyzer.[17] Because of the increased experimental energy resolution of $\Delta E = 25$ meV a more detailed energy loss peak structure can be observed and definite mode assignments are possible. A comparison of the experimental data with the results of a calculation based on a simple forced harmonic oscillator model[18] indicates that the spectrum is dominated by the excitation of the 3 IR-active normal modes ν_7 (117.6 meV), ν_{12} (179.0 meV), and ν_9 (385.0 meV) and their combinations. Table I shows that these have the largest IR intensities. The calculated spectrum is able to give a good simulation of the experimental results. The model spectrum shows a more detailed peak structure suggesting that

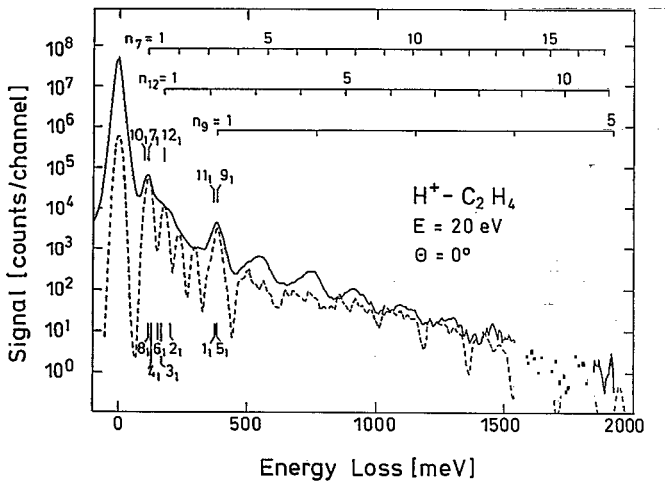

FIG. 3. PEL spectrum for C_2H_4 recorded at $E=20$ eV and $\theta=0°$ with an overall experimental resolution of 25 meV. The energies were scanned with a channel width of 5 meV. The experimental PEL spectrum (solid line) is compared with a simulated spectrum (dashed line) based on a simple forced harmonic oscillator model. The simulated spectrum was calculated using the 3 most dominant modes ν_7 (117.6 meV), ν_{12} (179.0 meV) and ν_9 (385.0 meV) and has been convoluted with the experimental resolution. The ladder scales in the upper part indicate the vibrational overtone states of these modes. The energy levels of the 12 normal mode fundamentals in C_2H_4 are marked by vertical lines. The levels marked above the spectrum correspond to the 5 IR-active modes, whereas the levels indicated below are the 7 IR-inactive modes.

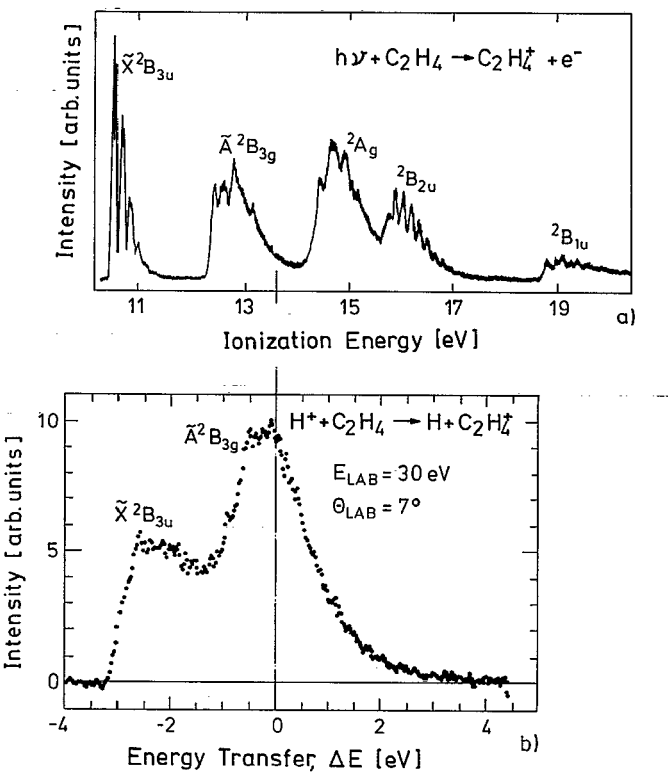

FIG. 4. Comparison of a photoionization spectrum (Ref. 19) (a) with a proton impact charge transfer energy transfer spectrum (b) for C_2H_4 at $E_{lab}=30$ eV and $\theta_{lab}=7°$. The energy scales in the spectra are the same and have been shifted so that 13.6 eV, the difference in energy between photoionization and proton charge transfer, in (a) corresponds to $\Delta E=0$ in (b).

some of the smearing of the experimental spectra may be due to additional contributions from other C_2H_4 normal modes. The energy position of the normal mode fundamentals are indicated by vertical lines in Fig. 3. Therefore the excitation of the IR-active ν_{10} or ν_{11} and of the IR-inactive ν_{2-}, ν_{3-}, or ν_6 mode and their combinations, in addition to the modes mentioned before, seems to be possible. The identification of the fundamental peaks will be discussed in more detail in a following section.

In Fig. 4, the charge transfer H-atom time-of-flight spectrum measured at a fairly large scattering angle of $\theta=7°$ is compared with a photoelectron time-of-flight spectrum[19] on the same energy transfer scale. The spectra are positioned such that the ionization thresholds lie directly underneath one another. This facilitates the assignment of the electronic levels produced in CT, namely, the ground $\tilde{X}\,^2B_{3u}$ and first excited $\tilde{A}\,^2B_{3g}$ electronic states, formed by removal of a C–C π and H–C–H σ bonding electron, respectively.

The intensity distributions in the two spectra are quite different from one another. In the photoelectron spectrum the electronic states are well separated and some vibrational structure can be identified. The overall shape of the CT spectrum can be understood by recalling that the probability of charge transfer is greatest when reactants and products are in energy resonance and decreases as the resonance condition is no longer fulfilled. Thus, in the first approximation, the CT energy transfer distribution can be explained by folding the photoelectron spectrum with a Gaussian distribution centered at $\Delta E=0$. This effect was clearly seen in an analogous study of charge transfer in H^+–H_2O collisions.[3,20] In the C_2H_4 spectra there appear to be some deviations from this simple model.

For one, the edges seen in the photoelectron spectrum for the $\tilde{X}\,^2B_{3u}$ and $\tilde{A}\,^2B_{3g}$ states at about 10.6 and 12.4 eV, respectively, are not nearly as sharp in the CT energy transfer spectrum as in the photoelectron spectrum. As seen in Fig. 4, the contribution from the $\tilde{A}\,^2B_{3g}$ state falls off at about $\Delta E=-1.2$ eV in accord with the photoelectron spectrum in Fig. 4(a). Thus we can assign the area under the spectrum at more negative energy transfers to the ground state and the remainder to the excited state.

There is no structure corresponding to excitation of the ^2A_g or the higher lying ^2B states in the photoelectron spectrum. In a study of the $H^+ + Xe$ system,[21] it was seen that much higher collision energies are required to significantly populate electronically excited states lying above the $\Delta E=0$ level. The $H^+ + C_2H_2$ system also showed no evidence for formation of electronically excited acetylene states. However, these structures may be contained within the $\tilde{A}\,^2B_{3g}$ feature especially at higher scattering angles (see Fig. 5). Because these levels cannot be separated from the $\tilde{A}\,^2B_{3g}$ contribution, in our subsequent data analysis all of the intensity observed for $\Delta E>0$ in the CT spectrum is simply attributed to high vibrational excitation within the $C_2H_4^+$ $\tilde{A}\,^2B_{3g}$ and $\tilde{X}\,^2B_{3u}$ states. Unfortunately, no vibrationally resolved spectrum could be obtained for the charge transfer process.

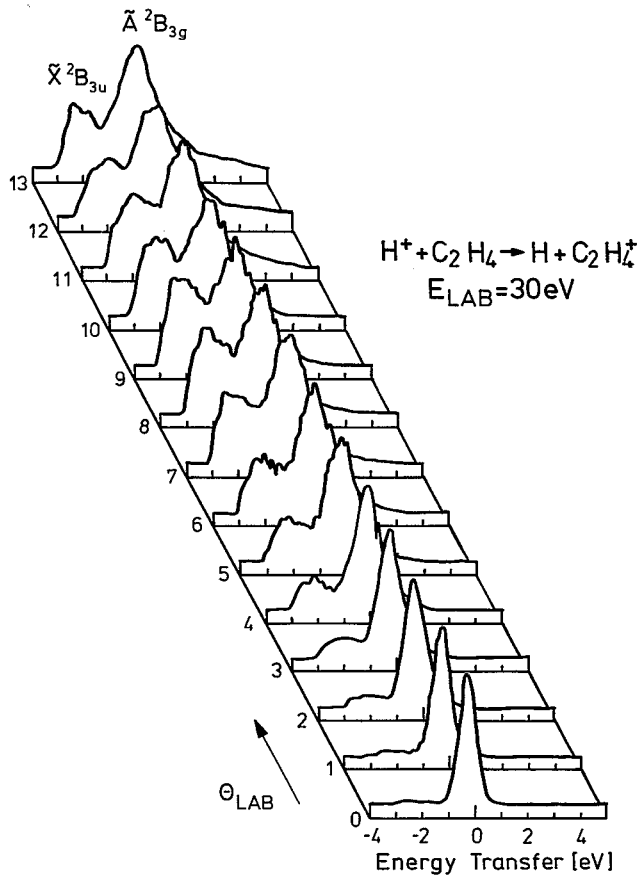

FIG. 5. Energy transfer distributions in charge transfer collisions at E_{lab} =30 eV collision energy at scattering angles up to θ=13°. At small scattering angles the resonant charge transfer into the electronically excited $\tilde{A}\,^2B_{3g}$ state dominates. With increasing scattering angle the contribution from charge transfer into the ground state $\tilde{X}\,^2B_{2u}$ increases.

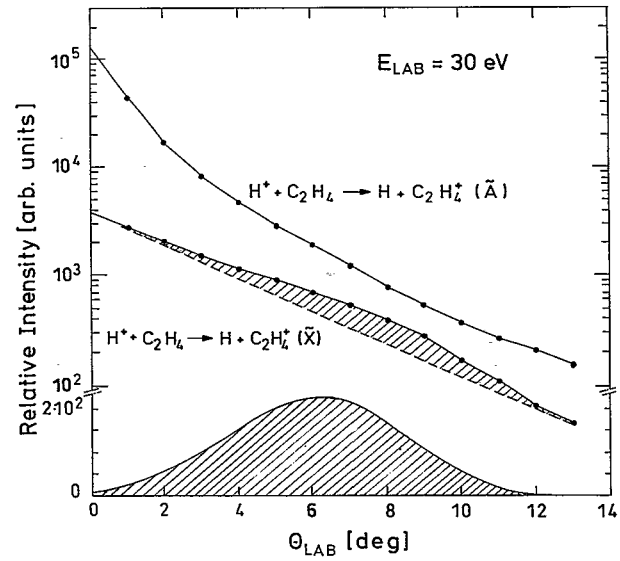

FIG. 6. Comparison of the relative intensities of H atoms in the two energy loss peaks attributed to C_2H_4 ions in the electronically excited $\tilde{A}\,^2B_{3g}$ and the $\tilde{X}\,^2B_{3u}$ ground state as seen in the spectra of Fig. 5. For the lower $\tilde{X}$ state curve the rainbow structure has been extracted by subtracting off a smooth extrapolation of the background to yield the shaded area. This is shown at the bottom on a linear intensity scale revealing a rainbow at about 6.5 degrees.

A theoretical analysis of the photoelectron spectrum[22] led to the conclusion that whereas the band due to the $\tilde{X}$ state can be resolved into separate vibrational modes or combination bands, the $\tilde{A}$ band contains $\simeq$1000 lines due to vibronic coupling at a conical intersection of the two states. This could account for the lack of vibrational resolution in the $\tilde{A}$ state, but the reason for the smearing of the vibrational structure in the $\tilde{X}$ state is not clear.

The relative probability of charge transfer into the two ionic electronic states can be seen from the time-of-flight spectra of H atoms measured as a function of scattering angle as shown in Fig. 5. In forward scattering, for $\theta \leqslant 2°$ only the energy resonant excited state, $\Delta E=0$, is produced in these long range collisions. Production of the $\tilde{A}$ state is always more probable than that of the $\tilde{X}$ state. We attribute this to the fact that it is quasiresonant, whereas the $\tilde{X}$ state is formed exothermically. As the collisions get closer, the intensity of the ground state with respect to the $\tilde{A}$ state increases to a maximum near $\theta=6.5°$, after which it again decreases. Simultaneously, as in IS, both peaks broaden indicating increasing vibrational excitation.

As Fig. 5 shows, above $\theta=5°$ there is substantial overlap between the two peaks. Thus, above this angle the data in Fig. 6 are best seen as a lower limit for the ground state cross section and an upper limit for production of the excited state. With this in mind, we have determined the partial differential charge transfer cross sections for the two states, derived from the following equations:

$$\frac{d\sigma_A(\theta)}{d\Omega}=\frac{S(\theta)}{[1+R(\theta)]}, \tag{1}$$

$$\frac{d\sigma_X(\theta)}{d\Omega}=\frac{S(\theta)}{[1+1/R(\theta)]}, \tag{2}$$

where $R(\theta)$ is the ratio of the total integrated ground state to total integrated excited state signal and $S(\theta)$ is their sum.

As shown in Fig. 6, the intensities of the $\tilde{A}$ and $\tilde{X}$ states decrease toward larger angles. The ground state curve shows what appears to be a slight maximum in the region between 6 and 10 deg. This maximum cannot be entirely due to the way in which the peak overlap was treated as discussed above. The resulting errors are estimated to be about 25% in this angular region. Rather we attribute it to a rainbow. To determine its location we have substracted off a smooth extrapolation of the background. The difference, presented at the bottom of Fig. 6 in a linear intensity plot, reveals a rainbow which is peaked at about $\theta_{RB}=6.5$ degrees. Using a relationship for the rainbow for ion-molecule systems $\epsilon=\Theta_{RB}E_i/1.7$ established earlier[23] we estimate a well depth of about $\epsilon=2.0\pm0.2$ eV.

Similar rainbows have also been distinctly observed in endothermic charge transfer processes in $H^+ + Kr$ (Ref. 21) and $H^+ + CO_2$ (Ref. 2), but not in exothermic CT in $H^+ + C_2H_2$ (Ref. 5). It was also seen in exothermic CT in

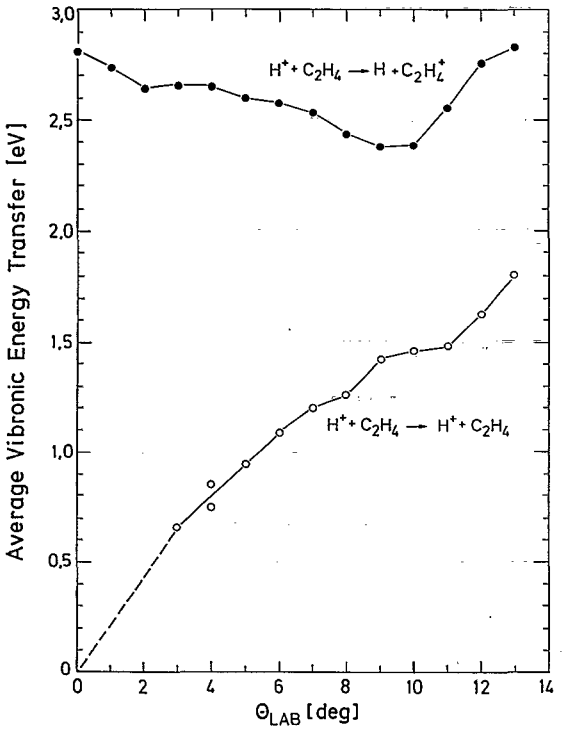

FIG. 7. Average internal energy transfer in charge transfer (filled circles) and in inelastic scattering (open circles). Note that at scattering angles greater than $\theta_{lab}=10°$ both processes show a parallel increase in energy transfer with increasing scattering angle.

TABLE II. Choices of coordinate systems for ethylene and corresponding symmetry representations of molecular orbitals and vibrational modes.

Reference	This work and Ref. 26	Refs. 12 and 25	Refs. 27 and 28
Molecular plane	yz	xy	xz
C–C bond axis	z	x	z
Axis ⊥ to molecular plane	x	z	y
Molecular orbitals			
$\pi_{u\parallel}$	b_{2u}	b_{2u}	b_{3u}
σ_g	a_g	a_g	a_g
$\pi_{g\parallel}$	b_{3g}	b_{1g}	b_{2g}
$\pi_{u\perp}$	b_{3u}	b_{1u}	b_{2u}
$\pi_{g\perp}$	b_{2g}	b_{2g}	b_{3g}
Vibrational modes			
$\nu_{1,2,3}$	a_g	a_g	a_g
ν_4	a_u	a_u	a_u
$\nu_{5,6}$	b_{3g}	b_{1g}	b_{2g}
ν_7	b_{3u}	b_{1u}	b_{2u}
ν_8	b_{2g}	b_{2g}	b_{3g}
$\nu_{9,10}$	b_{2u}	b_{2u}	b_{3u}
$\nu_{11,12}$	b_{1u}	b_{3u}	b_{1u}

$H^+ + CH_4$ (Ref. 4) and in a preliminary study of exothermically produced CH_3OH^+, where the ground state also showed a rainbow while the excited state did not.[20] This suggests that the observation of a rainbow implying the presence of an attractive well in the collision averaged potential has not only to do with the energetics of the process but also with other parameters, namely, the symmetry of the states involved, as will be shown below.

Despite the lack of resolution of final vibrational states, meaningful information can be obtained on the inelastic processes by determining the average internal energy transfer calculated from

$$\langle \Delta E(\theta) \rangle = \int P(\Delta E,\theta) \Delta E \cdot d\Delta E, \tag{3}$$

where $P(\Delta E,\theta)$ is the normalized measured energy loss probability distribution. The results for the IS and CT channels are shown in Fig. 7. The data have been analyzed in such a way that 0 eV energy transfer corresponds to production of neutral ground state C_2H_4 (open circles) or the ground state $C_2H_4^+$ ion (filled circles) in $v=0$. The curve for inelastic scattering shows a linear rise also observed previously for many systems and resulting from the increased momentum transfer with increasing angle. The energy transfer is somewhat smaller than in $H^+ + CH_4$ (Ref. 4) and slightly more than twice as high than observed for $H^+ + C_2H_2$ (Ref. 5). Thus, it does not appear to be related to the number of degrees of freedom in the system[24] but rather to other factors which will be discussed below. The large amount of energy transfered in CT is a result of the energy resonance in the charge transfer process. Unlike C_2H_2 which showed practically no angular dependence, for ethylene there is a relatively small decrease in ΔE up to about 9° which is somewhat greater than the rainbow angle and then a sharp increase. The initial decrease is directly related to the increase in the relative probability of forming the ground state product ion with scattering angle. For the very close collisions from the repulsive potential wall appearing beyond the rainbow angle, the energy transfer increases presumably because of strong impulsive interactions.

IV. DYNAMICAL APPROXIMATIONS

Before beginning the discussion we would like to clarify the great profusion of choices of molecular coordinates used for ethylene in the literature. This profusion seems to stem from the two conventions of either having z denote the axis of highest symmetry or an axis perpendicular to the molecule in the xy plane. Table II describes the coordinate system and symmetry representations used here and compares them with other conventions found in the literature. Our choice of coordinates places the ethylene molecule in the yz plane with z being the principal C–C axis (Fig. 8) and leads to the mode symmetry designations used in Table I. This is the convention adopted by Herzberg in Vol. III of his series, *Electronic Structure of Polyatomic Molecules*[25] which is different from the convention used in Vol. II *Infrared and Raman Spectra*.[26] Our numbering of the vibrations follows that of Ref. 26 but the symmetry designations are different. This is in order to achieve consistency in the vibrational and electronic designations.

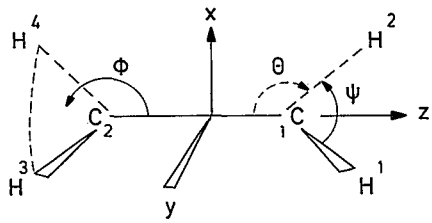

FIG. 8. Coordinate system of ethylene used in the present study. The molecule is in the *yz* plane and the C–C π bond is in the *xz* plane. The values of bond lengths and bond angles are in Table IV of the Appendix.

We would also like to alert the reader to the fact that the traditional nomenclature for two of the vibrations is not systematic: ν_5 is classified as *g* (gerade) and called *antisymmetric* and ν_{11}, although *u* (ungerade), is called *symmetric*.[26] Because our results are consistent with the systematic nomenclature, that is, *g* for symmetric and *u* for antisymmetric modes, in Table I we have changed the notation from that used in Ref. 26. In addition, counterintuitively, "rock" refers to an in-plane vibration whereas "wags" are out of plane.

In discussing the scattering of protons from ethylene, we assume that the angular motion of the proton (that is, the motion perpendicular to the vector *R* between the proton and the center of mass of ethylene) can be neglected and that the dynamics are determined by the motion along *R* alone. That is, we assume that the outcome of the collision is governed by the symmetry of the system at the point of closest approach where *R* is a minimum. In the small angle grazing collisions of interest here, this approximation of a straight line trajectory is quite reasonable.[4,5,14] Additional simplifying assumptions are needed because of the many vibrational degrees of freedom. For this reason a full scattering calculation cannot be envisaged for the near future. Thus the theoretical discussion of the observed differential cross sections and vibronic distributions is based, as in our previous reports, only on general symmetry considerations and a qualitative view of the potential energy surfaces. Therefore we will discuss the results in terms of the mechanisms mentioned in the Introduction, namely, the induced dipole mechanism for small angle scattering and large impact parameters and the internal vibronic mechanism for larger scattering angles and closer collisions.

To perform the simple symmetry analysis, some assumptions have to be made about the temporary collision complex. For example, in our study of C_2H_2, two idealized situations of perpendicular (C_{2v}) and collinear ($D_{\infty h}$) attack were made. In this work we prefer to consider the more general case where the movement of the projectile is confined to the molecular *yz* plane or the *xz* plane which is perpendicular to it rather than to a particular high-symmetry axis. In Fig. 9, we show the potential energy surfaces involved in this system in the two collision geometries of C_s^{xz} and C_s^{yz}. These two sets of potential curves were estimated from the asymptotic energies taken from the literature.[10] From the proton affinity we estimate that the $H^+ + C_2H_4$ reactants lead diabatically to a deep well of $\simeq$6.9 eV of ethyl ion.[29] We do not make any assumptions about the $C_2H_5^+$ structure at the bottom of the well, i.e., whether it is "classical" (ethyl ion) or "nonclassical" (an ethylene with the proton bridging the carbon–carbon double bond). The two charge transfer product surfaces are primarily repulsive since the polarizability of H is small

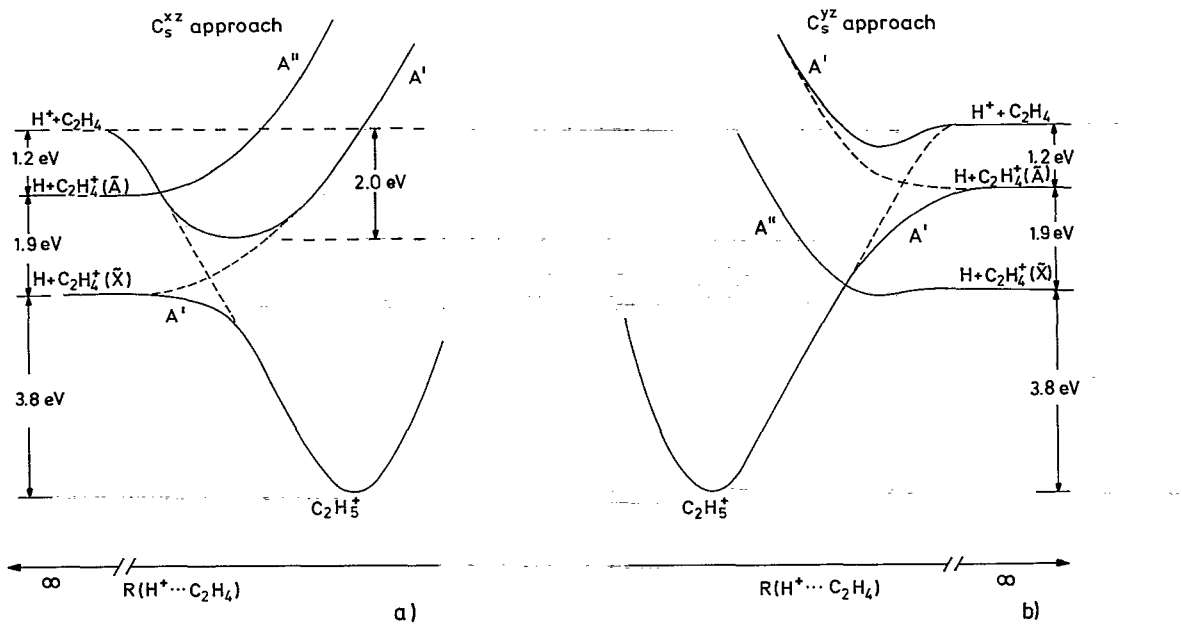

FIG. 9. Potential energy surface diagrams for $(H\cdots C_2H_4)^+$ in (a) C_s^{xz} and (b) C_s^{yz} collision geometries. No specific structure is assigned to the protonated species at the bottom of the well. The asymptotic energies and the well depth of 6.9 eV (Ref. 29) are taken from the literature. The units on the radial coordinate are arbitrary. The solid lines show the adiabatic surfaces while the diabatic potentials are indicated by the dashed lines.

TABLE III. Correlation of irreducible representations. Ground state of ethylene is D_{2h}.

Point group:	D_{2h}	C_s^{xz}	C_s^{yz}	C_{2v}^{x}	C_{2v}^{y}	D_2	C_2^x
	a_g	a'	a'	a_1	a_1	a	a
	b_{1g}	a''	a''	b_1	b_2	b_1	b
	b_{2g}	a'	a''	b_2	a_2	b_2	b
	b_{3g}	a''	a'	a_2	b_1	b_3	a
	a_u	a''	a''	a_2	a_2	a	a
	b_{1u}	a'	a'	b_2	b_1	b_1	b
	b_{2u}	a''	a'	b_1	a_1	b_2	b
	b_{3u}	a'	a''	a_1	b_2	b_3	a

and the ion-induced dipole potential is shallow.

To simplify the following discussion, we have provided the correlations between the irreducible representations of various point groups in Table III. This allows easy switching from the D_{2h} description of an isolated ethylene molecule to the C_s^{xz} or C_s^{yz} classification used in Fig. 9. (The C_{2v} and D_2 configurations are discussed in the Appendix.)

A. Large impact parameters (induced dipole mechanism)

At the largest impact parameter collisions corresponding to small scattering angles, we expect the excitation to be driven by IDM involving only the long range electrostatic ion-molecule interactions. These will be strongest for vibrational modes of the molecule which have a nonzero dipole moment derivative, which are the infrared-active, antisymmetric modes. The infrared intensities for these vibrations are known and also listed in Table I. Neglecting for the moment resonance effects, to be discussed below, we expect from the infrared intensities that the ν_7 peak at 118 meV should be the strongest, ν_9 at 385 meV to be the second most intense, ν_{11} and ν_{12} at 370 and 179 meV, respectively, to be the third strongest and of about equal intensity, and ν_{10} at 102 meV to be hardly visible. The experimental results in Fig. 3 show a strong excitation of the ν_7 mode which agrees well with the predicted peak intensities. However, instead of the ν_9 mode, the ν_{12} mode, lying between contributions from the IR-inactive ν_2 and ν_3 or ν_6 modes, is found to be the second most intense. Although the infrared intensity of ν_{12} is much weaker compared to ν_9 its vibrational period $[\tau_{\text{vib}}(\nu_{12}) \approx 2.3 \cdot 10^{-14}$ s] is closer to the known resonance condition $\tau_{\text{coll}} \approx 1/2\tau_{\text{vib}}(\tau_{\text{coll}} \approx 1 \cdot 10^{-14}$ s at $E=20$ eV) which enhances the T–V energy transfer.[1] Contributions from the other two IR-active modes ν_{10} and ν_{11} are less probable because of the low infrared intensity (ν_{10}) or the shorter vibrational period (ν_{11}), respectively.

The presence of features in Fig. 3 due to dipole inactive modes ν_2, ν_3, or ν_6 could in principle be attributed to ion–quadrupole interactions.[18] However, such an effect should be much weaker than ion–dipole coupling since it has an R^{-3} rather than an R^{-2} dependence. An additional mechanism, such as the vibronic mixing discussed in the Introduction and described in detail below, can also be responsible for these features.

At large intermolecular separations the efficiency of charge transfer is controlled by the degree of resonance of the H^+–C_2H_4 and H–$C_2H_4^+$ surfaces. Charge transfer into the $\tilde{A}$ state of the ionic ethylene is favored over the ground state because of the smaller energy difference to the reactants. Since no vibrationally resolved spectrum of the charge transfer products is expected due to the strong vibronic interaction at the conical intersection that exists with the ground state surface of the ion,[22] we have no information on which vibrational modes are the most strongly excited in these collisions.

B. Smaller impact parameters (internal vibronic mechanism)

In closer collisions the system begins to probe the regions of the surface crossings and the system begins to resemble more a $C_2H_5^+$ complex. Therefore, the collision geometry can play a role in the selection of the vibrational modes to be excited.

The diagram in Fig. 9 shows that the reactants and the excited state charge transfer product surfaces have different electronic symmetries in C_s^{xz} (A' and A'') and the same in C_s^{yz} (both A'). Thus, in C_s^{xz} a crossing is allowed and, nominally, no interaction between the surfaces takes place. In C_s^{yz} repulsion between the diabatic surfaces is indicated by the solid lines as an avoided crossing.

Looking at the correlations in Table III and then inspecting the available modes in Table I, we see that this implies excitation of all except for the twist and the wag modes. Most importantly, it is consistent with the observation of the symmetric C–C stretch (ν_2) and CH_2 scissor (ν_3) modes in Fig. 3 which, despite the lack of resolution in Fig. 2, can be seen to become more intense with increasing θ. The forces leading to excitation of these modes can be explained by recalling that the $\tilde{A}$ state of the ethylene ion is formed by removing an electron from a primarily H–C–H bonding and C–C antibonding orbital. The proliferation of possible excitations explains the loss of resolution in the IS spectra of Fig. 2 toward larger scattering angles as the vibronic coupling mechanism becomes important.

Note that the C_s^{xz} collision geometry can also lead to vibrational excitation or charge transfer through the IVM. In this case we can induce an interaction between the two electronic surfaces by mixing in vibrational modes that make the total symmetry become the same, $a' \times a'' = a''$. This then constrains the crossing to also become avoided. In other words, excitation of any a'' mode in C_s^{xz} symmetry distorts the complex to facilitate IS and CT. Again looking at Tables III and I, we see that this implies excitation of C–H stretches ν_5 and ν_9, the two rocks ν_6 and ν_{10}, and the twist ν_4. Presumably the C–H stretches will be the strongest promoters of CT in view of the ionization of the $\tilde{A}$ state requiring removal of an electron from a bonding H–C–H orbital, as mentioned above. Excitation of the rock modes is less likely as evidenced by the data in Fig. 3.

In still closer collisions the reactant diabatic surface crosses the diabatic ground state charge transfer product surface. Here the situation is just the reverse from the

above, the crossing is avoided in C_s^{xz} symmetry and allowed in C_s^{yz}. All the arguments are the same as above with interchange of a' and a''. Thus, combining both the C_s^{xz} and C_s^{yz} collision geometries, most vibrational modes of the ground state ion can be excited to some degree. Along with the interaction with the $\tilde{A}$ state through the conical intersection mentioned above, this is possibly why no single vibrational modes could be resolved in the ground state envelope in Fig. 4.

A more detailed analysis of the observations has to take into account the differences in the adiabatic potential curves for the two geometries. The avoided crossing in the C_s^{xz} approach leads to an interaction via a strongly attractive potential well with a depth which we estimate from the experiment to be about 2.0 eV. In the C_s^{yz} approach the avoided crossing leads to a much weaker adiabatic potential well. Thus the trajectories in the C_s^{yz} geometry will be more repulsive than in the C_s^{xz} approach and consequently most of the trajectories at angles up to the rainbow in the vicinity of 6° have passed through the C_s^{xz} geometry. The link between the rainbow scattering and the two geometries is also apparent from the energy transfer distributions in Fig. 5. There it is seen that the probability for excitation of the $\tilde{X}$ state rises from a plateau of small probability at angles between $\theta_{lab}=4$ and 7° to another plateau of large probability which is altogether consistent with this picture. The overall smaller probability of $\tilde{X}$ production at large angles is, of course, due to the larger energy difference and thus does not invalidate our arguments about the propensity for the C_s^{xz} geometry at low scattering angles.

It is interesting to speculate about the reason for the minimum between 9° and 10° in the $\tilde{X}$-state energy transfer seen in Fig. 7. One possible explanation is suggested by considering a network of vibronic states as shown schematically in Fig. 10. Of course we realize that in the high velocity regime we cannot think in terms of adiabatic states. However, Child[30] has shown that when the collision time becomes very short the dynamical couplings can still be discussed in similar terms as in the adiabatic case. It is also justified to still use the Landau–Zener model in which the probability of a diabatic passage through the network is given by

$$P_{dia}=\exp(-kH^2/v_{\|}\,\Delta F),$$

where k is a constant, H is one half of the energy splitting between the corresponding two adiabatic surfaces, $v_{\|}$ is the effective collision velocity, and ΔF is the difference in slopes of the diabatic surfaces at the effective crossing point.

If we associate $v_{\|}$ with the velocity along the distance between the proton and the center of mass of C_2H_4 then we expect $v_{\|}$, and thus P_{dia}, to increase with decreasing impact parameter corresponding to increasing scattering angles. We can restrict ourselves to considering the C_s^{xz} geometry because of the strong coupling, not present in C_s^{yz}. Three scenarios can be identified. (1) At small angles the trajectories tend to remain on the diabatic curves and those that ultimately undergo a curve crossing do not have much vibrational excitation. (2) This effect is extreme just at the

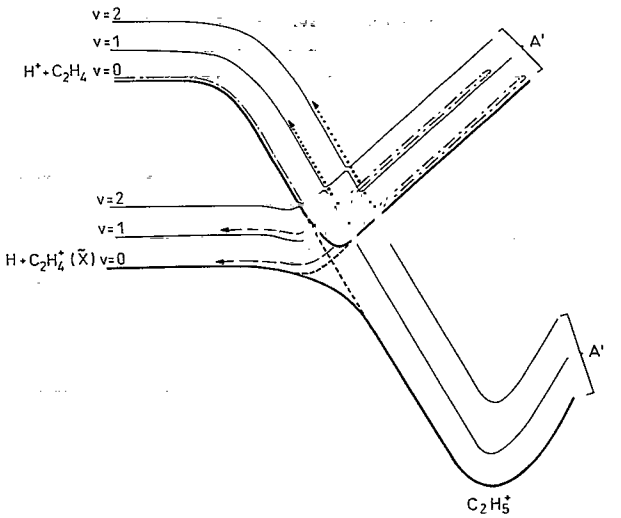

FIG. 10. Vibronic network for C_2^{xz} approach (not to scale). Showing schematically the vibronic levels involved in the crossing of the H^+–C_2H_4 and H–$C_2H_4^+$($\tilde{X}$) potential curves. For simplicity the potential curves for the H–$C_2H_4^+$(A) system have been left out. Thick lines are the same adiabatic surfaces as in Fig. 9. Thin lines are overtones of an *arbitary* vibronic mode. Dashed lines are pathways which result in charge transfer, dotted lines are pathways for inelastic scattering.

rainbow angle when many trajectories reach the bottom part of the crossing between vibronic curves of $H^+ + C_2H_4$ and $H + C_2H_4^+$ A' networks. This accounts for the minimum at 9°–10° (which, to be sure, is at a somewhat larger angle than the rainbow at 6.5°). (3) Then with a further decrease in impact parameter those trajectories which cross over into the repulsive branch of the $H + C_2H_4^+(\tilde{X})$ curves now have to pass through another set of crossings on the way back. They thus have a higher probability of undergoing crossings leading to more vibrational excitation in the $C_2H_4^+(\tilde{X})$ molecular ion.

Finally it is interesting to apply similar considerations to explain the absence of an angular dependence in ΔE for CT in the proton–acetylene system despite the presence of a potential well seen in the IS data. In this very exothermic process the crossing points between vibronic levels are at small proton-C_2H_2 separations where the slopes of the potential energy surfaces are steep. Even though the spacing between vibronic levels is large, the radial position of the crossings does not shift by very much from level to level. Therefore, trajectories leading to products in different vibronic levels still experience similar deflection angles because they feel similar potentials. This explains not only the angular independence of the amount of energy transfer but also the low efficiency of excitation of acetylene, which requires close collisions.

V. CONCLUSIONS

All features in the observed angular and time-of-flight distributions of scattered protons and H atoms resulting in collisions of protons with ethylene can be explained in terms of two interaction schemes: At large impact parameters, a long range ion–dipole mechanism promotes excita-

tion of the infrared active vibrational modes in the molecule and near-resonant charge transfer. The intensities of the peaks in the proton time-of-flight spectrum correspond to vibrational modes of the molecule and are in agreement with the known infrared intensities. In closer collisions, a short range symmetry dependent internal vibronic mechanism, incorporating vibronic mixing at a crossing of the available reactant and charge transfer product potential surfaces, accounts for the observed excitation of infrared inactive vibrational modes. As the collisions get closer, individual vibrational lines in the time-of-flight distributions of inelastically scattered protons can no longer be separated from one another. This is attributed to the low symmetry of the $C_2H_5^+$ system which allows nearly all vibronic modes to be coupled at the crossing.

Two of the electronic states of $C_2H_4^+$ $\tilde{X}\,^2B_{3u}$ and $\tilde{A}\,^2B_{3g}$ are resolved in the time-of-flight spectra of the H-atom charge transfer product; however no vibrational levels could be resolved even at the smallest scattering angles. This is attributed to the interaction between these two electronic states of the C_2H_4 ion at a conical intersection.[22] However, the angular distributions did reveal that the upper state $\tilde{A}$, which is near resonant with the reactants, can be formed at large impact parameters, whereas the ground state $\tilde{X}$ requires closer collisions. The efficiency of forming the ground state ethylene ion rises relative to that of the excited state with scattering angle. A shoulder in the angular distribution of the ground state is attributed to rainbow scattering caused by a $\simeq$2.0 eV potential well. These phenomena are interpreted by examining the two possible collision symmetries of a qualitative potential energy surface. When the proton approaches in the molecular plane, there is an avoided crossing between the reactant and *excited* state charge transfer product surface. When the proton approaches perpendicular to the molecular plane, there is an avoided crossing between the reactant and the *ground state* charge transfer product surface. This accounts both for the electronic state dependence in the angular distribution of the charge transfer process as well as the potential well.

Finally, the average amount of internal energy transfer in charge transfer also shows a small minimum in the angular dependence. This is explained in terms of the probability of passing through diabatic crossings between interacting vibronic states as a function of the relative velocity along the direction of approach, which is directly correlated to the impact parameter, as is the scattering angle.

Further details of the excitation mechanisms based on idealized behavior of the system at low energy and long collision times, i.e., in the limit that the collision complex can find its highest symmetry configuration, are given in the Appendix. This discussion gives a more refined picture of the various interactions based on vibronic coupling arguments. Such an interpretation is expected to be useful to model future experiments performed at higher resolution and lower collision energies.

ACKNOWLEDGMENTS

Y.N.C. wishes to dedicate his contribution to the late Professor Robert S. Mulliken. It was in Professor Mulliken's laboratory in 1962 that Y.N.C. first learned about nonadiabatic effects in diatomic molecules. Y.N.C. thanks J. P. Toennies and his colleagues for their hospitality and enthusiastic discussions during his stay in Germany. We also thank Dr. Thomas Glenewinkel–Meyer for enlightening discussions.

APPENDIX: VIBRATIONAL EXCITATION MECHANISMS

In Sec. IV, we have considered the vibrational excitation for proton approach to ethylene on two orthogonal planes on which the valence orbitals $1b_{3u}$ and $1b_{3g}$ lie. These are the orbitals from which an electron is extracted in the course of charge transfer. A better approximation to the random orientation of the target molecule with respect to the incoming projectile H^+ is achieved by describing the collision on a plane rather than on a single line in the plane. While the linear combination of these two planes will cover the three-dimensional encounter of the scatter-

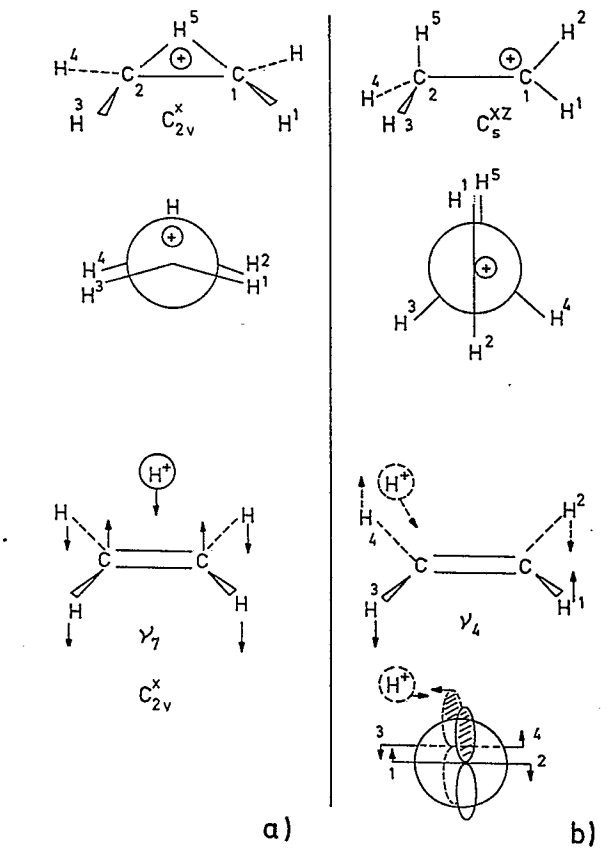

FIG. 11. High symmetry $C_2H_5^+$ geometries which can lead to temporarily stable complexes. The bottom portion of the figure shows the direction of proton approach and the distortion of neutral ethylene on the way to complex formation. (a) The "nonclassical" bridged structure. The proton approaches along the x axis and excites primarily the ν_7 wag. (b) The twisted ethyl ion, whose production is promoted by the twisting ν_4 vibration. The proton approaches in the xz plane nearer to one end of the C–C bond than the other. The bend of the CH_2 group contributes to the excitation of the ν_8 wag.

TABLE IV. Comparison of molecular coordinates (geometric distortion) and orbital excitation energies affecting vibrational excitation. Bond lengths in Angstroms, bond angles in degrees. See Fig. 8 for the definition of the molecular coordinates. Only the most strongly affected parameters are considered in each row.

Vibration	Predominant molecular coordinate involved	C_2H_4 (^1A_g)[a]	$C_2H_4^+$ ($\tilde{X}\,^2B_{3u}$)[b]	$C_2H_4^+$ ($\tilde{A}\,^2B_{3g}$)[c]	$C_2H_5^+$ (C_{2v}^{α})[d]	$C_2H_5^+$ (C_s)[d]	Orbital excitation energies of C_2H_4[e]
ν_1	r(C–H)	1.076		> 1.076	1.074	1.107	
$\nu_2(\nu_{1,3})$	r(C–C)	1.330	> 1.330		1.375	1.443	
ν_3	ψ(H–C–H)	116.6			117.8		
ν_4							
ν_5	r(C–H)	1.076		> 1.076	1.329	1.088	
ν_6	$\theta(H_2$–CC–$H_2)$	121.7				120.8	
ν_7	$\phi(H_2$–CC–$H_2)$	180			176.8	180	7.2 eV($\pi\sigma^*$)
ν_8	$\phi(H_2$–CC–$H_2)$	180			176.8	121	7.2 eV($\pi\sigma^*$,$\sigma\pi^*$)
ν_9	r(C–H)	1.076		> 1.076	1.074	1.107	
ν_{10}	$\theta(H_2$–CC–$H_2)$	121.7			123		
ν_{11}	r(C–H)	1.076		> 1.076	1.074	1.077	5.5 eV($\pi\pi^*$)
ν_{12}	ψ(H–C–H)	116.6			117.8		5.5 eV($\pi\pi^*$)

[a]Ground state ethylene geometry is used as the reference point from which the degree of distortion in the course of ionization or complex formation is measured. Values from Ref. 31.
[b]Removal of a π_{ux} electron in ionization of ethylene will weaken the C–C bond.
[c]Removal of a π_{gy} electron in ionization of ethylene will weaken the C–H_2 bonds.
[d]Values from Refs. 35, 37, and 38.
[e]The affected vibrations have the same symmetries as the excited electronic states of ethylene. Values from Ref. 28.

ing objects, it does not take full advantage of the high symmetry of the ethylene. Because of the high energy of the proton beam (30 eV), we also did not discuss the possibility for the system to follow the lowest energy adiabatic path leading to complex formation.

In this Appendix, we give a comprehensive account of all possible encounters, in particular those of high symmetry which lead to formation of stable $C_2H_5^+$ geometries, namely, the bridged complex and the ethyl ion, Fig. 11. From these, the excitation of specific ethylene and ethylene ion modes can be easily visualized. Such a discussion is appropriate for low collision energies in the chemical domain allowing closer encounters and probing the bottoms of potential wells. The purpose of this treatment is to thoroughly elaborate and compile predictions for future experiments. While this Appendix strives to be comprehensive and self contained, for completeness, some discussion on details already discussed will be necessary.

For this system there are five mechanisms for vibrational energy transfer, which operate with or without charge transfer. These different mechanisms dominate under different scattering conditions. We shall enumerate all of them. Finally, we shall summarize their contributions for comparison with present and future experiments. The mechanisms are: For lower scattering angles and longer range interaction (1) infrared allowed transitions due to the charge-induced dipole potential (IDM) and (2) internal vibronic coupling in near-resonant charge transfer to the first excited ionic state $\tilde{A}(^2B_{3g})$ (IVM). For large scattering angles and short range interactions (3) internal vibronic coupling in exothermic charge transfer to the ground state $\tilde{X}(^2B_{3u})$ (IVM), (4) $C_2H_5^+$ formation accompanied by bond dilution and structural deformation, and (5) second-order Jahn–Teller coupling in the quasimolecular complex (QMM).

Table IV summarizes the factors that are expected to affect vibrational excitation the most, dipole and quadru-

TABLE V. Probability of vibrational excitation with the proposed mechanism. Only relative intensities across the same row or down the same column should be compared. The results of zero excitation probability for a given mode, except for the IDM mechanism are the most rigorous, being governed by symmetry. The expected intensities are indicated by the number of stars: ***** is very strong, **** strong *** moderately strong, ** medium, * weak.

	IDM C_2H_4 (^1A_g)	Charge transfer $C_2H_4^+$ ($\tilde{X},^2B_{3u}$)	$C_2H_4^+$ ($\tilde{A},^2B_{3g}$)	QMM $C_2H_5^+$ (C_{2v}^{α})	$C_2H_5^+$ (C_s)
ν_1		***		**	**
ν_2		****		**	***
ν_3		***		**	**
ν_4		****			****
ν_5		*	****		
ν_6		*	**		**
ν_7	*****	***		****	**
ν_8					***
ν_9	****				
ν_{10}	*				*
ν_{11}	***		***		***
ν_{12}	***		*		****

pole derivatives, and geometrical distortions.[31] These parameters, along with IR and Raman intensities, are used to derive the qualitative ranking of the vibrational excitation probabilities given in Table V.

1. IDM

This is the classical mechanism due to the radiation field of the moving proton, as discussed above.[14] The dipole allowed modes are ν_{11} and $\nu_{12}(b_{1u})$ polarized along z, the ν_9 and $\nu_{10}(b_{2u})$ polarized along y, and $\nu_7(b_{3u})$ polarized along x. Experimental as well as theoretical values for the change of dipole moment are known and are proportional to the infrared transition intensities.[13]

2. IVM (excited ionic state)

To produce the excited $C_2H_4^+$ $\tilde{A}$ state from C_2H_4, an electron is abstracted from the occupied $\pi_{gy}(1b_{3g})$ orbital which is antibonding in C–C but bonding in C–H. It is therefore reasonable to assume that in the lowest energy path the proton approaches in the CH_2 plane which is also the molecular yz plane. This was noted in the Discussion and in Fig. 9. In the special case that the proton approaches along the y axis the symmetry that is conserved for the charge transfer reaction producing the planar excited state ion is C_{2v}^y. We will discuss the vibrational excitations that can occur when the proton is constrained to approach in this symmetry.

The product electronic state B_{3g} in D_{2h} correlates to B_1 in C_{2v}^y, and the reactants, of course, to A_1 (Table III). Nominally, there is no interaction between the two electronic surfaces. But by mixing in of vibrations that conserve the total symmetry between products and reactants, i.e., $A_1 \times B_1 = b_1$ modes, the *vibronic* surfaces can mix, leading to an avoided crossing and hence, to nonzero charge transfer probabilities. The vibrations that have such symmetry are the ν_5 and ν_6 (both b_{3g}), and the ν_{11} and ν_{12} (both b_{1u}). The ν_5 C–H stretch is the most logical response to the bond dilution of the C–H bonds on the side where the proton approaches. Similarly, the $\nu_{11}CH_2$ stretch also responds to the weakening of the C–H bonding. Excitation of the ν_6 rock and ν_{12} scissor would seem to be minor effects.

By virtue of the twisting vibration ν_4, ions of the $\tilde{A}$ state can make a rapid transition (within the time scale of a collisional encounter of femtoseconds) into the ground twisted state via a conical intersection.[11,22,32,33] Therefore the vibrations detected in the ion will be "broadened" by the uncertainty principle (Fig. 4). This broadening is so strong that no assignment of the vibrational modes is feasible.[22]

Although we have discussed only the charge transfer channel, we should note that the same mechanism holds for the inelastic scattering channel and leads to an analogous excitation pattern. In this case, a temporary charge transfer state is produced during which the excitation takes place. The end products, however, retain the initial reactant electronic configuration.

We now turn to mechanisms that operate at smaller impact parameters and lead to products at large scattering angles.

3. IVM (twisted ground state ion)

This process occurs at small impact parameters with deep penetration of the potential and thus has a small cross section at larger scattering angles (Fig. 5). Before reaching the "bottom" of the $\tilde{X}$ potential, the molecular ion can still be approximated as being planar. Therefore, proton approach on the xz plane conserves C_s^{xz} symmetry. This is the treatment used in the Discussion, justified by the high-energy regime of the experiment.

If the collision energy were low enough so that the system could probe deeper into the $C_2H_5^+$ well, then charge transfer must lead to a twisted ionic state which serves as a symmetry trap for certain vibrations.[32,33] These vibrations, primarily the twisting ν_4 mode, will be enhanced in the product ion.

We let the proton approach along the x axis to abstract an electron from the highest occupied molecular orbital $\pi_{ux}(b_{3u})$. Then the symmetry group that can describe both the planar reactant and the twisted product is C_2^x, in which both species are in the A representation. Vibrational modes that also belong to the A representation, and thus will be most strongly affected, are the ν_1 to ν_7.[34] Of these, the ν_4 can be most distinctly seen to prepare the system for transition from reactant to twisted product. Excitation of the other vibrations, all of which have a component of C–C stretch,[26] is due to the dilution of the C–C bond by the charge withdrawal of the proton.

4. $C_2H_5^+$ formation

In this mechanism, the reacting system forms a quasimolecule as the proton probes the potential of the $C_2H_5^+$ complex. There is only one stable complex among the many studied, the "nonclassical" bridged structure.[35–38] This configuration has been found to be 6.3 kcal/mol lower in energy than the ethyl ion with twisted CH_2 planes, which sits at a saddle point in the potential surface (rotational transition structure).[38]

Formation of a given structure can be seen as the result of a particular direction of approach of the proton. For each complex geometry, bond dilution and structural deformation lead to unique symmetry-dependent preferences for vibrational excitation.

a. Nonclassical bridged structure

Approach on the xz plane may lead to the bridged complex provided that the proton energy is such that the system can take the adiabatic low energy path into the potential well. Of course, the most efficient means to produce this ion is by aiming the proton directly at the center of the C–C π_{ux} orbital. The symmetry group that describes the system now is C_{2v}^x. Reactants and products are totally symmetric in this configuration and thus belong to the A_1 representation. Looking at Tables III and I, we see that vibrational modes that are also in a_1 symmetry are the ν_1, ν_2, and ν_3 stretches and the ν_7 wag. One can certainly

expect that the C–C bond will be stretched upon complex formation. The ν_7 promotes electron transfer to the approaching proton by yielding up the π orbital electrons as well as bending the CH_2 groups away to make more room. This is illustrated in Fig. 11(a).

b. Rotational transition structure

In this structure the two CH_2 planes are twisted with respect to each other. The extra proton may be visualized at one end of the C–C bond, for example, on the *xz* plane as in Fig. 11(b). It causes the CH_2 at this end to flap down below the *yz* plane. Clearly formation of this structure will involve excitation of the ν_4 twist as well as the ν_8 wag. Because there are no further symmetry restrictions, other modes resulting from dilution of the C–C bond (ν_1,ν_2,ν_3) and from geometrical distortion (ν_7,ν_{11},ν_{12}), are also possible.

5. QMM

This mechanism has been discussed in our previous publications.[4,5,17] As the proton hovers near the molecule, the excited state surface might be lowered in energy as they progress toward a bonding interaction to form the quasimolecule. (This may even result in points of degeneracy between the excited state surface and the charge-transfer products leading to efficient resonant charge transfer). This decrease in the splitting increases the probability that these high-lying states will endow the ground state C_2H_4 with vibrations of the same symmetry as the excited state via a second order Jahn–Teller effect. The probability amplitude or coefficient of mixing is

$$a=\langle\psi_i\chi_m^0|\partial H/\partial Q_m\cdot Q_m|\psi_j\chi_m^1\rangle/|E_i-E_j|,$$

where ψ and χ are the electronic and vibrational wave functions, respectively. The indexes i and j (m) denote the symmetries of different electronic states (vibrational modes), and the superscripts 0 and 1 indicate the number of vibrational quanta. As for IVM, the modes that will be affected by this mechanism conserve the total symmetry, namely, $\Gamma_i=\Gamma_j\times\Gamma_m$, where Γ is the irreducible representation of the electronic or vibrational symmetry.

For C_2H_4 the excited states in question are the $^1B_{1u}(...1b_{3u}1b_{2g}$, $\pi-\pi^*$ state) at 5.5 eV, $^1B_{3u}(...1b_{3u}4a_g$, $\pi-\sigma^*$ state) at 7.1 eV, and $^1B_{2g}(...1b_{3u}3b_{1u}$, $\pi-\sigma^*$ mixed with $3a_g1b_{2g}$, $\sigma-\pi^*$ state) at 7.2 eV. Upon twist, the $^1B_{1u}$ state decreases in energy and becomes $^1B_1$ of D_2 and the $^1B_{3u}$ and $^1B_{2g}$ become $^1B_3$ and $^1B_2$ and approach degeneracy at 90°. Clearly, because of the denominator term, E_i-E_j, the probability amplitude for mixing in the lower energy states is greater. Thus, the ν_{11} and ν_{12} vibrations of b_{1u} symmetry will be more strongly affected by this mechanism, than those of $b_{3u}(\nu_7)$ and $b_{2g}(\nu_8)$ symmetries. Interestingly, except for ν_8 these are the same vibrations that are affected in IDM and will thus enhance the effects of that mechanism.

[1] G. Niedner-Schatteburg and J. P. Toennies, in *State-Selected and State-to-State Ion-Molecule Reaction Dynamics, Part I: Experiment*, edited by Cheuk-Yiu Ng and Michael Baer, Advances in Chemical Physics Series, Vol. LXXXII (Wiley, New York, 1992), p. 553.
[2] M. Noll and J. P. Toennies. J. Chem. Phys. **85**, 3313 (1986); G. Niedner, M. Noll, and J. P. Toennies, *ibid.* **87**, 2067 (1987); G. Niedner, M. Noll, J. P. Toennies, and C. Schlier, *ibid.* **87**, 2685 (1987); F. A. Gianturco, U. Gierz, and J. P. Toennies, J. Phys. B **14**, 667 (1981).
[3] B. Friedrich, G. Niedner, M. Noll, and J. P. Toennies, J. Chem. Phys. **87**, 5256 (1987).
[4] Y.-N. Chiu, B. Friedrich, W. Maring, G. Niedner, M. Noll, and J. P. Toennies, J. Chem. Phys. **88**, 6814 (1988).
[5] N. Aristov, G. Niedner, J. P. Toennies, and Y.-N. Chiu, J. Chem. Phys. **95**, 7969 (1991).
[6] M. W. Crofton, M. F. Jagod, B. D. Rehfuss, and T. Oka, J. Chem. Phys. **86**, 3755 (1987).
[7] R. Unwin, H. H. Rotermund, A. M. Bradshaw, and W. Peatman, Annual Report of the Berlin Synchrotron Facility BESSY, 193, 1989.
[8] Y.-N. Chiu, J. Phys. Chem. **92**, 4352 (1988).
[9] I. B. Bersuker and V. Z. Polinger, *Vibronic Interaction in Molecules and Crystals*, Springer Ser. Chem. Phys. Vol. 49 (Springer, Heidelberg, 1989).
[10] R. Stockbauer and M. G. Inghram, J. Chem. Phys. **62**, 4862 (1975).
[11] G. Sannen, G. Raseev, C. Galloy, G. Fauville, and J. C. Lorquet, J. Chem. Phys. **74**, 2402 (1981).
[12] G. P. Raine and H. F. Schaefer III, J. Chem. Phys. **81**, 4034 (1984).
[13] A. Komornicki and J. W. McIver, Jr., J. Chem. Phys. **70**, 2014 (1979).
[14] U. Gierz, M. Noll, and J. P. Toennies, J. Chem. Phys. **82**, 217 (1985).
[15] J. A. Ray, C. F. Barnett, and B. von Zyl, J. Appl. Phys. **50**, 6516 (1979).
[16] From the measured relative cross section for quasi-resonant charge transfer the relative efficiency for H atom detection efficiency was estimated to be only 1%. See M. Baer, R. Düren, B. Friederich, G. Niedner, M. Noll, and J. P. Toennies, Phys. Rev. A **36**, 1063 (1987).
[17] W. Maring, J. P. Toennies, R. G. Wang, and H. Levene, Chem. Phys. Lett. **184**, 262 (1991); W. Maring, Dissertation, University of Göttingen, 1991.
[18] T. Ellenbrock and J. P. Toennies, Chem. Phys. **71**, 309 (1982).
[19] K. Kimura, S. Katsumata, Y. Achiba, T. Yamazaki, and S. Iwata, *Handbook of He (I) Photoelectron Spectra of Fundamental Organic Molecules* (Japan Scientific Societies, Tokyo, 1981).
[20] G. Niedner, Dissertation, University of Göttingen, 1988, Max-Planck-Institut für Strömungsforschung, Report No. 13/1988.
[21] M. Baer, R. Düren, B. Friedrich, G. Niedner, M. Noll, and J. P. Toennies, Phys. Rev. A **36**, 1063 (1987).
[22] H. Köppel, L. S. Cederbaum, and W. Domcke, J. Chem. Phys. **77**, 2014 (1982).
[23] G. D. Barg, G. M. Kendall, and J. P. Toennies, Chem. Phys. **16**, 243 (1976).
[24] W. Eastes and J. P. Toennies, J. Chem. Phys. **70**, 1644 (1979).
[25] G. Herzberg, *Electronic Spectra and Electronic Structure of Polyatomic Molecules* (Van Nostrand, Princeton, 1967).
[26] G. Herzberg, *Infrared and Raman Spectra of Polyatomic Molecules* (Van Nostrand Reinhold, New York, 1945).
[27] R. E. Ballard, *Photoelectron Spectroscopy and Molecular Orbital Theory* (Adam Hilger, London, 1978).
[28] R. S. Mulliken and W. C. Ermler, *Polyatomic Molecules. Results of Ab initio Calculations* (Academic, New York, 1981).
[29] F. A. Houle and J. L. Beauchamp, J. Am. Chem. Soc. **101**, 4067 (1979).
[30] M. S. Child, *Molecular Collision Theory* (Academic, London, 1974).
[31] R. Ditchfield, W. J. Hehre, and J. A. Pople, J. Chem. Phys. **54**, 724 (1971).
[32] H. Köppel, W. Domcke, L. S. Cederbaum, and W. von Niessen, J. Chem. Phys. **69**, 4252 (1978).
[33] H. Köppel, L. S. Cederbaum, W. Domcke, and S. S. Shaik, Angew. Chem. **22**, 210 (1983).
[34] Y.-N. Chiu and M. Gong. Chem. Phys. **131**, 191 (1989).
[35] P. C. Hariharan, W. A. Latham, and J. A. Pople, Chem. Phys. Lett. **14**, 385 (1972).
[36] J. A. Pople, Int. J. Mass Spectrosc. Ion Phys. **19**, 89 (1976).
[37] H. Lischka and J. J. Köhler, J. Am. Chem. Soc. **100**, 5297 (1978).
[38] K. Raghavachari, R. A. Whiteside, J. A. Pople, and P. V. R. Schleyer, J. Am. Chem. Soc. **103**, 5649 (1981).